Supplementary Materials of Random Noise Defense against Query-Based Black-Box Attacks

Zeyu Qin[1] **Yanbo Fan**[2] **Hongyuan Zha**[1] **Baoyuan Wu**[1†]
[1]School of Data Science, Shenzhen Research Institute of Big Data,
The Chinese University of Hong Kong, Shenzhen
[2]Tencent AI Lab
zeyuqin@link.cuhk.edu.cn, fanyanbo0124@gmail.com,
zhahy@cuhk.edu.cn, wubaoyuan@cuhk.edu.cn

In this supplementary document, we provide additional materials to supplement our main submission. In Section A, we talk about the societal impacts of our work In Section B, we provide detailed experimental settings as well as further evaluation results on CIFAR-10 and ImageNet. We also provide the comparison with input transformation-based defense methods. In Section D, we give the proofs *w.r.t.* Theorem 1 of the main submission. In Section E, we give the proofs *w.r.t.* Theorem 2 of the main submission. The proofs of Theorem 3 are given in Section F.

In Section C, we provide the analysis and evaluation of decision-based attacks.

A Societal Impacts

Deep neural networks (DNNs) have been successfully applied in many safety-critical tasks, such as autonomous driving, face recognition and verification, *etc*. And adversarial samples have posed a serious threat to machine learning systems. For real-world applications, the DNN model as well as the training dataset, are often hidden from users. Instead, only the model feedback for each query (*e.g.*, labels or confidence scores) are accessible. In this case, the product providers mainly face the severe threats from query-based black-box attacks, which don't require any knowledge about the attacked models. In this work, we study a lightweight defense method RND against query-based black-box attacks. We conduct the detailed theoretical and empirical analysis of performance of RND against query-based black-box attacks. Extensive experiments verify our theoretical analysis and show the effectiveness of our defense methods against several state-of-the-art query-based attacks. Besides, RND can be directly combined with any off-the-shelf models and other defense strategies.

Therefore, RND is efficient and effective to defend query-based black-box attacks in real scenarios. Without any extra modification, RND can be add to deployed machine learning systems to boost the adversarial robustness.

[†]Corresponding author.

35th Conference on Neural Information Processing Systems (NeurIPS 2021).

B Experiments

We conduct all experiments on 2 Nvidia-V100 GPU. And we run all experiments 3 times and average all results over 3 random seeds.

RND is very easy to implemented. The defenders add one line code in the Pytorch framework [22], x = x + noise_size * torch.randn_like(x). noise_size is the ν used in main submission. In inference time, the defenders adopt this method after image transformations and before normalization.

B.1 Implementation Details of Black-Box Methods

The CIFAR-10 dataset contains 60,000 32×32 color images in 10 different classes, which can be seperated into 50,000 training samples and 10,000 testing samples. These two datasets are licensed under MIT. ImageNet contains 1,000 classes with 1.28 million images for training and 50k images for validation. Imagenet is licensed under Custom (non-commercial).

We evaluate seven mainstreamed query-based attack methods: NES [16], ZOsignSGD [18], Bandit Prior [17], SimBA [13], SignHunter [1], ECO [20], and Square attack [2]. For NES, ZOsignSGD, Bandit Prior, SimBA, and SignHunter, we adopt the source code provided by the authors of SignHunter [1]. For Square attack, we use the source code provided by the authers [2]. For ECO, we adopt the source code provided by the authors [3]. For Signhunter, we only evaluate it under the ℓ_∞ attack, since its performance under the ℓ_2 attack is worse than NES [1]. SimBA is only designed for ℓ_2 attack. For all attacks, we adopt the hyperparameters recommended by the corresponding papers, which are also shown in Table 1-7. For the evaluation on ImageNet, we use the randomly sampled 1000 images provided by [15][4].

B.2 Implementation Details of Compared Methods

We compare our methods with adversarial training (AT) [11, 12], Feature Denoise [26], RSE [19] and PNI [14]. For AT model, we adopt the pre-trained WideResNet-28-10 AT model [5] in CIFAR-10. It utilizes the extra unlabeled data. For ImageNet, we adopt the pre-trained ResNet-50 AT model in Robustness Library [6]. It's trained with $4/255$ ℓ_∞ attack. For Feature Denoise, we adopt the pre-trained ResNet-152 model [7]. For RSE and PNI, we use source code [8] [9] provided by the authors to train the corresponding WideResNet-28-10 models. For standard training VGG model and WideResNet models in CIFAR-10, we use the codes [10] [11] to train them. For used models on ImageNet, we adopt the pre-trained checkpoints provided by *torchvision*.

B.3 Implementation Details of Gaussian Augmentation Fine-tuning

For GF model, on CIFAR-10, we fine-tune WideResNet-28-10 model with random Gaussian noise sampled from $\mathcal{N}(\mathbf{0}, 0.1\mathbf{I})$. We use the SGD optimizer with momentum 0.9 and weight decay $5 * 10^{-4}$ We used a variation of the learning rate schedule from [24] to achieve superconvergence in 50 epochs, which is piecewise linear from 0 to 0.001 over the first 20 epochs, down to 0.0005 over the next 20 epochs, and finally back down to 0 in the last 10 epochs.

On ImageNet, [23] released the ResNet-50 model fine-tuned with Gaussian noise sampled from $\mathcal{N}(\mathbf{0}, 0.5\mathbf{I})$ and we directly adopt it.

[1] https://github.com/ash-aldujaili/blackbox-adv-examples-signhunter

[2] https://github.com/max-andr/square-attack

[3] https://github.com/snu-mllab/parsimonious-blackbox-attack

[4] https://github.com/TransEmbedBA/TREMBA

[5] https://github.com/deepmind/deepmind-research/tree/master/adversarial_robustness

[6] https://github.com/MadryLab/robustness

[7] https://github.com/facebookresearch/ImageNet-Adversarial-Training

[8] https://github.com/xuanqing94/BayesianDefense

[9] https://github.com/elliothe/CVPR_2019_PNI

[10] https://github.com/kuangliu/pytorch-cifar

[11] https://github.com/DengpanFu/RobustAdversarialNetwork

Table 1: Hyperparameters setup for NES

	CIFAR-10		ImageNet	
	ℓ_∞	ℓ_2	ℓ_∞	ℓ_2
Hyperparameter				
η (learning rate)	0.01	0.25	0.005	1
q (number of finite difference estimations per step)	30		60	

Table 2: Hyperparameters setup for ZOsignSGD (ZS)

	CIFAR-10		ImageNet	
	ℓ_∞	ℓ_2	ℓ_∞	ℓ_2
Hyperparameter				
η (learning rate)	0.01	0.20	0.005	0.1
q (number of finite difference estimations per step)	30		60	

Table 3: Hyperparameters setup for Bandit Prior

	CIFAR-10		ImageNet	
	ℓ_∞	ℓ_2	ℓ_∞	ℓ_2
Hyperparameter				
η (learning rate)	0.01	0.25	0.01	0.5
h (OCO learning rate)	0.1		0.0001	
δ (Bandit exploration)	0.1		0.1	
Tile Size (Data-dependent prior)	20		50	

Table 4: Hyperparameters setup for SimBA

	CIFAR-10	ImageNet
	ℓ_2	ℓ_2
Hyperparameter		
η (step size)	0.2	0.2

Table 5: Hyperparameters setup for SignHunter

	CIFAR-10	ImageNet
	ℓ_∞	ℓ_∞
Hyperparameter		
η (step size)	0.05	0.05

Table 6: Hyperparameters setup for Square Attack (Square)

	CIFAR-10		ImageNet	
	ℓ_∞	ℓ_2	ℓ_∞	ℓ_2
Hyperparameter				
μ (Fraction of Pixel Changed)	$0.05 \sim 0.5$		$0.05 \sim 0.5$	

Table 7: Hyperparameters setup for ECO

	CIFAR-10	ImageNet
	ℓ_∞	ℓ_∞
Hyperparameter		
block size	4	16
block batch size	64	64

B.4 Additional experimental results of Section 5.2

Experimental results of RND against Query-based ℓ_2 Attacks. Here we provide the defense performance of RND with various settings of μ and ν against query-based black-box ℓ_2 attack. We adopt the same parameter setting as ℓ_∞ attack. Figure 1 (a-d) and Figure 2 (a-d) present the defense performance of RND with VGG-16 and WideResNet-16 against NES, ZS, Bandit and Square attack on CIFAR-10, respectively. The experimental results on ImageNet are shown in Figure 3 (a-d). From the results, **we have similar observations with that against ℓ_∞ attack**: 1) When $\nu = 0.0$ (i.e., without RND), the attack failure rate of all ℓ_2 attack methods is very low at all values of μ and ν, which verifies the poor robustness of the standard model against the query-based attacks. 2) For RND with $\nu > 0$, the attack failure rate of all attack methods generally increases as the value of $\frac{\nu}{\mu}$ increases. While for a certain value of μ (0.0001 or 0.001 for ZO attacks and 0.1 or 0.3 for Square attack), the attack failure rate increases as the value of ν increases. These verify our theoretical analysis that the ratio of $\frac{\nu}{\mu}$ determines the upper bound of the convergence rate of query-based ZO attacks and the probability of changing the sign. The larger the value of $\frac{\nu}{\mu}$ results in the poorer attack performance under the query-limited settings. The evaluations in terms of average and median number of queries of successful attacks are shown in Table 8-16, respectively. For brevity, we only report the numerical results with $\mu \in \{0.0001, 0.001, 0.01\}$ for ZO attacks and $\mu \in \{0.1, 0.3, 0.5\}$ for Square attack. And, we set $\nu \in \{0.0, 0.01, 0.02\}$. From the table, we can see that the average query number and the median query number of successful attacks increases as the ratio of $\frac{\nu}{\mu}$ increases. Thus RND can improve the defense performance by increasing the attack failure rate and reducing the query efficiency of black-box attacks. The results of RND with $\mu = 0.0001, 0.0005, 0.001, 0.005, 0.01$ under ℓ_∞-attack on ImageNet is also provided in Figure 4.

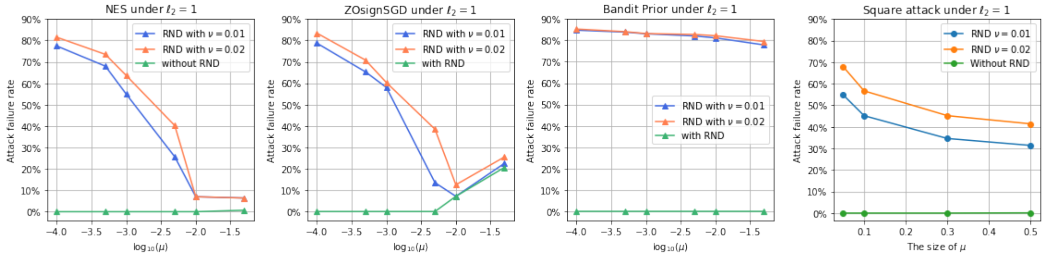

(a) (b) (c) (d)

Figure 1: Attack failure rate (%) of query-based attacks on WideResNet-16 and CIFAR-10 under different values of μ and ν. We adopt logarithm scale in subplot (a-c) for better illustration.

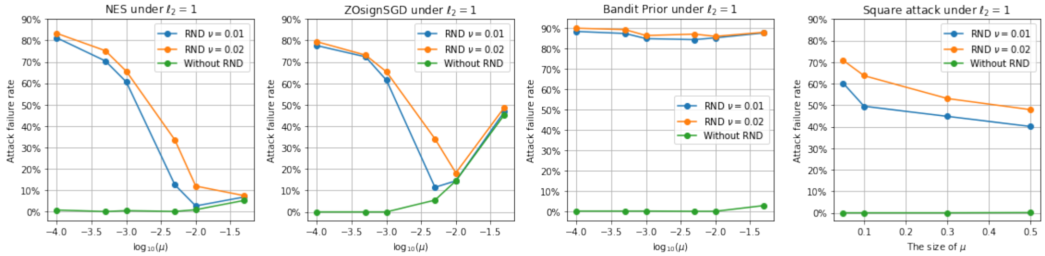

(a) (b) (c) (d)

Figure 2: Attack failure rate (%) of query-based attacks on VGG-16 and CIFAR-10 under different values of μ and ν. We adopt logarithm scale in subplot (a-c) for better illustration.

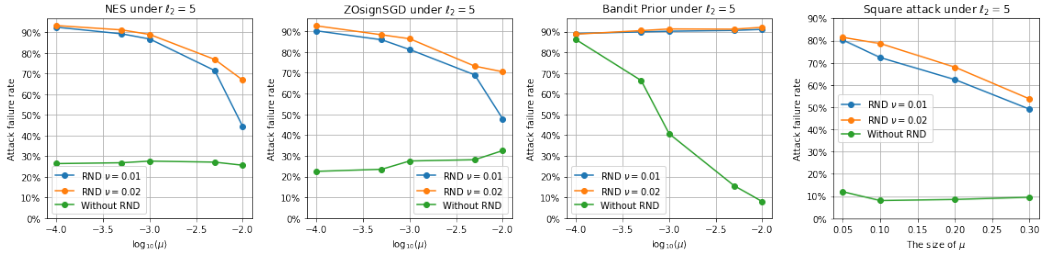

(a) (b) (c) (d)

Figure 3: Attack failure rate (%) of query-based attacks on Inception v3 and ImageNet under different values of μ and ν. We adopt logarithm scale in subplot (a-c) for better illustration.

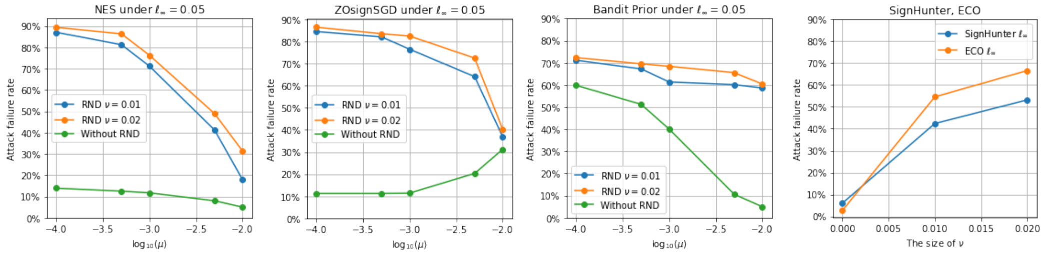

(a) (b) (c) (d)

Figure 4: Attack failure rate ($\%$) of query-based attacks on Inception v3 and ImageNet under different values of μ and ν. We adopt logarithm scale in subplot (a-c) for better illustration.

Table 8: The experimental results of NES, ZS, and Bandit attack on CIFAR-10, VGG-16 model. Each value in this table means the average number of query of successful attack, the median of query, and failure rate $\in [0, 1]$.

Methods \ μ/ν	$10^{-4}/0.0$	$10^{-4}/0.01$	$10^{-4}/0.02$	$10^{-3}/0.0$	$10^{-3}/0.01$	$10^{-3}/0.02$	$10^{-2}/0.0$	$10^{-2}/0.01$	$10^{-2}/0.02$
NES (ℓ_∞)	281.0(180.0)/0.0	1602.2(570.0)/0.621	1660.3(580.0)/0.688	280.3(180.0)/0.0	1506.0(600.0)/0.437	1448.4(510.0)/0.484	267.3(180.0)/0.0	398.8(220.0)/0.0	693.4(330.0)/0.06
NES (ℓ_2)	380.2(30.0)/0.0	1981.4(810.0)/0.812	1974.2(760.0)/0.833	378.5(300.0)/0.0	1987.7(900.0)/0.606	1792.2(690.0)/0.656	374.8(270.0)/0.0	626.3(360.0)/0.03	1009.1(480.0)/0.12
ZOsignSGD (ℓ_∞)	246.8(155.0)/0.0	1707.4(620.0)/0.00	1729.1(627.0)/0.702	257.4(155.0)/0.00	1499.6(558.0)/0.485	1489.7(496.0)/0.493	342.4(155.0)/0.0	493.9(240.0)/0.03	828.8(372.0)/0.1
ZOsignSGD (ℓ_2)	337.0(275.0)/0.0	2249.0(868.0)/0.776	1785.6(744.0)/0.794	340.1(275.0)/0.0	1939.0(1147.0)/0.615	1851.8(899.0)/0.654	452.8(310.0)/0.145	706.1(465.0)/0.158	1254.7(682.0)/0.182
Bandit (ℓ_∞)	117.7(56.0)/0.00	402.5(20.0)/0.744	410.8(20.0)/0.768	115.8(52.0)/0.0	382.5(18.0)/0.677	436.4(21.0)/0.696	111.3(54.0)/0.0	168.4(36.0)/0.58	183.6(32.0)/0.622
Bandit (ℓ_2)	394.1(186.0)/0.0	987.2(820.0)/0.885	1000.4(80.0)/0.901	389.1(190.0)/0.0	981.9(82.0)/0.850	967.2(83.0)/0.865	393.0(182.0)/0.0	919.6(102.0)/0.854	912.4(100.0)/0.861

Table 9: The experimental results of Square attack on CIFAR-10, VGG-16 model. Each value in this table means the average number of query of successful attack, the median of query, and failure rate $\in [0, 1]$.

Methods \ μ/ν	0.1/0.0	0.1/0.01	0.1/0.02	0.3/0.0	0.3/0.01	0.3/0.02	0.5/0.0	0.5/0.01	0.5/0.02
Square (ℓ_∞)	64.7(26.0)/0.0	196.3(25.0)/0.152	194.9(12.0)/0.215	101.6(37.0)/0.0	203.9(26.0)/0.08	235.1(19.0)/0.134	150.9(60.0)/0.0	194.2(20.0)/0.04	261.4(33.0)/0.105
Square (ℓ_2)	407.1(160.0)/0.0	381.4(40.0)/0.495	695.1(46.0)/0.637	470.4(199.0)/0.0	687.7(48.0)/0.448	552.9(54.0)/0.531	567.8(239.0)/0.0	626.3(60.0)/0.40	544.1(67.0)/0.479

Table 10: The experimental results of SignHunter, SimBA, and ECO on CIFAR-10, VGG-16 model. Each value in this table means the average number of query of successful attack, the median of query, and failure rate $\in [0, 1]$.

Methods \ ν	0.0	0.01	0.02
SignHunter (ℓ_∞)	106.8(570.0)/0.0	372.3(64.0)/0.208	459.2(55.0)/0.367
SimBA (ℓ_2)	308.0(136.0)/0.0	1707.4(623.0)/0.473	1352.8(172.0)/0.650
ECO (ℓ_∞)	207.5(146.0)/0.0	964.6(256.0)/0.609	904.3(232.0)/0.720

Table 11: The experimental results of NES, ZS, and Bandit attack on CIFAR-10, WideNet-16 model. Each value in this table means the average number of query of successful attack, the median of query, and failure rate $\in [0, 1]$.

Methods \ μ/ν	$10^{-4}/0.0$	$10^{-4}/0.01$	$10^{-4}/0.02$	$10^{-3}/0.0$	$10^{-3}/0.01$	$10^{-3}/0.02$	$10^{-2}/0.0$	$10^{-2}/0.01$	$10^{-2}/0.02$
NES (ℓ_∞)	265.5(180.0)/0.00	1692.5(480.0)/0.606	1702.0(570.0)/0.645	250.4(180.0)/0.00	1626.0(630.0)/0.389	1572.8(570.0)/0.434	264.8(180)/0.0	352.6(210.0)/0.0	731.9(330)/0.03
NES (ℓ_2)	368.4(270.0)/0.0	1942.9(720.0)/0.774	1735.8(800.0)/0.815	374.9(270.0)/0.0	2046.5(990.0)0.549	1715.1(750.0)/0.636	304.4(240.0)/0.0	550.0(330.0)/0.0	1115.7(510.0)/0.07
ZOsignSGD (ℓ_∞)	188.4(124.0)/0.0	1657.7(496.0)/0.591	1638.0(523.0)/0.642	191.0(124.0)/0.0	1477.0(620.0)/0.424	1447.3(496.0)/0.453	190.1(124.0)/0.0	436.7(217.0)/0.012	747.5(341.0)/0.065
ZOsignSGD (ℓ_2)	295.3(248.0)/0.0	2181.4(868.0)/0.787	2254.5(850.0)/0.834	296.1(248.0)/0.0	2156.6(1209.0)/0.580	2136.2(1312.0)/0.603	580(310.0)/0.008	772.8(434.0)/0.071	1237.4(744.0)/0.125
Bandit (ℓ_∞)	92.51(44.0)/0.0	108.1(30.00)/0.647	124.7(31.0)/0.672	90.76(42.0)/0.0	382.5(40.0)/0.602	401.6(39.0)/0.625	91.98(42.0)/0.0	214.8(43.0)/0.461	345.7(43.0)/0.486
Bandit (ℓ_2)	281.6(158.0)/0.0	1592.2(160.0)/0.848	1611.3(152.0)/0.853	282.3(158.0)/0.0	1595.8(160.0)/0.831	1621.3(160.0)/0.832	275.12(158.0)/0.0	973.0(84.0)/0.812	1125.0(78.0)/0.822

Table 12: The experimental results of Square attack on CIFAR-10, WideNet-16 model. Each value in this table means the average number of query of successful attack, the median of query, and failure rate $\in [0, 1]$.

Methods \ μ/ν	$0.1/0.0$	$0.1/0.01$	$0.1/0.02$	$0.3/0.0$	$0.3/0.01$	$0.3/0.02$	$0.5/0.0$	$0.5/0.01$	$0.5/0.02$
Square (ℓ_∞)	42.8(19.0)/0.0	185.1(27.0)/0.112	294.9(22.0)/0.190	121.6(27.0)/0.0	231.2(26.0)/0.08	245.2(19.0)/0.144	250.1(60.0)/0.0	294.2(23.0)/0.04	264.1(35.0)/0.105
Square (ℓ_2)	303.1(131.0)/0.0	964.3(103.0)/0.452	597.8(39.0)//0.567	293.4(131.0)/0.0	587.2(48.0)/0.346	589.4(61.0)/0.456	440.1(210.0)/0.0	626.3(60.0)/0.314	516.4(72.0)/0.414

Table 13: The experimental results of SignHunter, SimBA, and ECO on CIFAR-10, WideNet-16 model. Each value in this table means the average number of query of successful attack, the median of query, and failure rate $\in [0, 1]$.

Methods \ ν	0.0	0.01	0.02
SignHunter (ℓ_∞)	95.0(55.0)/0.0	415.7(56.0)/0.271	651.8(59.0)/0.396
SimBA (ℓ_2)	241.2(138.0)/0.0	1813.0(702.0)/0.476	1359.1(187.0)/0.648
ECO (ℓ_∞)	157.6(76.0)/0.0	787.4(236.0)/0.533	788.8(218.0)/0.637

Table 14: The experimental results of NES, ZS, and Bandit on ImageNet, Inception v3 model. Each value in this table means the average number of query of successful attack, the median of query, and failure rate $\in [0, 1]$.

Methods \ μ/ν	$10^{-4}/0.0$	$10^{-4}/0.01$	$10^{-4}/0.02$	$10^{-3}/0.0$	$10^{-3}/0.01$	$10^{-3}/0.02$	$10^{-2}/0.0$	$10^{-2}/0.01$	$10^{-2}/0.02$
NES (ℓ_∞)	1678.4(960.0)/0.139	3037.5(2040.0)/0.870	3010.6(2025.0)/0.893	1435.4(900.0)/0.117	3402.3(2280.0)/0.711	2532.8(1560.0)/0.762	1571.2(840.0)/0.05	1721.8(1080.0)/0.179	2143.4(1380.0)/0.313
NES (ℓ_2)	2016.5(1215.0)/0.264	1888.9(360.0)/0.925	1954.1(345.0)0.933	2021.1(1200.0)/0.276	2245.7(1200.0)/0.868	1814.2(720.0)/0.890	2048.6(1200.0)/0.256	1836.0(900.0)/0.444	2378.2(1440.0)/0.669
ZOsignSGD (ℓ_∞)	1312.9(671.0)/0.113	2232.6(1159.0)/0.845	1870.5(1132.0)/0.865	1316.7(671.0)/0.114	2244.3(1464.0)/0.771	2824.1(1586.0)/0.825	1544.2(793.0)/0.312	1678.5(1203.5)/0.334	2355.3(1708.0)/0.373
ZOsignSGD (ℓ_2)	1642.6(1350.0)/0.225	1389.9(445.0)/0.902	1389.9(427.0)/0.926	1442.6(1240.0)/0.275	1389.9(545.0)/0.812	1375.3(490.0)/0.864	1945.6(1100.0)/0.325	1745.6(985.0)/0.478	1245.4(785.0)/0.705
Bandit (ℓ_∞)	696.7(16.0)0.598	114.2(12.0)/0.711	122.5(12.0)/0.723	1422.6(104.0)/0.40	202.1(16.0)/0.613	195.4(16.0)/0.684	903.1(142.0)/0.050	288.4(18.0)/0.586	305.6(20.0)/0.604
Bandit (ℓ_2)	987.9(118.0)/0.861	583.6(60.0)0.891	656.4(42.0)/0.848	1483.5(990.0)/0.407	615.3(60.0)/0.902	578.6(60.0)/0.913	1327.2(636.0)/0.088	246.5(92.0)/0.911	235.2(91.0)/0.921

Table 15: The experimental results of Square attack on ImageNet, Inception v3 model. Each value in this table means the average number of query of successful attack, the median of query, and failure rate $\in [0, 1]$.

Methods \ μ/ν	$0.1/0.0$	$0.1/0.01$	$0.1/0.02$	$0.3/0.0$	$0.3/0.01$	$0.3/0.02$	$0.5/0.0$	$0.5/0.01$	$0.5/0.02$
Square (ℓ_∞)	247.1(23.0)/0.003	576.8(19.0)/0.149	207.4(18.0)/0.264	359.9(40.0)/0.05	339.6(25.0)/0.122	251.7(17.0)/0.207	457.0(66.0)/0.08	315.2(28.0)/0.106	296.3(16.0)/0.154
Square (ℓ_2)	1107.1(310.0)/0.08	1030.2(316.0)/0.723	997.8(390.0)//0.786	1247.5(409.0)/0.09	1187.2(480.0)/0.491	1089.4(461.0)/0.537	1340.1(510.0)/0.11	1226.3(460.0)/0.426	1236.4(480.0)/0.493

Table 16: The Experiment of SignHunter, SimBA, and ECO on ImageNet, Inception v3 model. Each value in this table means the average number of query of successful attack, the median of query, and failure rate $\in [0, 1]$.

Methods \ ν	0.0	0.01	0.02
SignHunter (ℓ_∞)	557.2(108.0)/0.056	163.4(50.0)/0.424	173.4(49.0)/0.532
SimBA (ℓ_2)	2077.4(1398.0)/0.195	223.6(21.0)/0.885	274.6(19.0)0.891
ECO (ℓ_∞)	853.2(258.0)/0.027	1043.2(485.0)/0.432	1236.9(691.0)/0.666

B.5 Additional experimental results of Section 5.3

Experimental results of RND against The Adaptive EOT Attack. We also evaluate the defense performance of RND against EOT with ℓ_2 attack. The evaluations with adaptive query budget on

NES and ZS of CIFAR-10 are shown in Table 19 and 20. From the Table, we observe that the attack failure rate decreases as M increases on both datasets. However, the average number of queries of successful attack also greatly increases as M increases, which demonstrates that the adaptive EOT attack increases the attacking success rate with a sacrifice of query efficiency. We also observe that the relative performance improvements induced by EOT under both ℓ_∞ and ℓ_2 attack generally decrease as M increases, especially when M is rather large. For example, for NES with ℓ_∞ attack, the relative improvement of $M = 20$ over that of $M = 15$ is only 0.004 in terms of attack failure rate. Yet the average query number of $M = 20$ is 306 higher than that of $M = 15$. These validate our theoretical analysis in Section 4.3 of the main submission that the attack improvement from EOT is limited as M increases.

The experimental results under the fixed query budget on CIFAR-10 and ImageNet are reported in Table 17 and 18, respectively. On these two datasets, the attack failure rate of all attacks generally decreases as M increases. Yet we also observe the similar phenomenon that the relative performance improvements induced by EOT decreases as M increases.

Table 17: The evaluation of EOT with ℓ_2 attack on CIFAR-10 under the fixed query budget setting. The average number of query of successful attack as well as the attack failure rate are reported. For all attacks, we set $\nu = 0.02$ and set $\mu = 0.001$ for NES, ZS, and Bandit. Each value in this table means the average number of query of successful attack, the median of query, and failure rate $\in [0, 1]$. The higher failure rate, the better defense performance.

Methods	M=1	M=5	M= 10
NES	1792/690/0.656	4736/2850/0.598	5167/3220/0.523
ZS	1939/1147/0.615	3921/3410/0.578	4135/4215/0.541
Bandit	912/100/0.861	662/160/0.782	698/193/0.745
Square	413/42/0.708	284/70/0.777	263/69/0.815
SimBA	1353/172/0.650	3852/1585/0.467	4103/2836/0.396

Table 18: The evaluation of EOT with ℓ_2 attack on ImageNet under the fixed query budget setting. The average number of queries of successful attack as well as the attack failure rate are reported.

Methods	M=0	M=5	M=10
NES	1814/0.890	4825.6/0.912	5801.3/0.925
ZS	1375/0.864	3055/0.887	4652/0.861
Bandit	195/0.684	698/0.579	873/0.0.553
Square	160.9/0.822	178.0/0.831	179.5/0.845
SimBA	274/0.891	468/0.878	517/0.869

Table 19: The evaluation of EOT with ℓ_∞ and ℓ_2 attack on CIFAR-10 under the adaptive query budget setting. The average number of queries of successful attack as well as the attack failure rate are reported. For all attacks, we choose the same parameter as the Table 17.

Datasets	Methods	M=1	M=5	M=10	M=15	M=20
CIFAR-10	NES(ℓ_∞)	1448/0.484	4078/0.361	5763/0.342	6126/0.331	6342/0.327
	NES(ℓ_2)	1792/0.656	3074/0.513	3642/0.456	4023/0.432	4125/0.429
	ZS(ℓ_∞)	1489/0.493	3189/0.354	5912/0.319	6159/0.293	7013/0.287
	ZS(ℓ_2)	1852/0.654	4052/0.541	4619/0.498	4923/0.475	4867/0.472

Table 20: The evaluation of EOT with ℓ_∞ attack on ImageNet under the adaptive query budget setting. The average number of queries of successful attack as well as the attack failure rate are reported. For all attacks, we still set ν as 0.02 and increase μ to 0.01.

Datasets	Methods	M=1	M=5	M=10	M=15
ImageNet	NES(ℓ_∞)	0.313	0.251	0.236	0.224
	NES(ℓ_2)	0.669	0.603	0.576	0.551
	ZS (ℓ_∞)	0.373	0.279	0.261	0.257
	ZS(ℓ_2)	0.705	0.616	0.579	0.556

B.6 Additional experimental results of Section 5.4

Experimental results of Compared Methods against ℓ_2 attack. We adopt the same experimental setting reported in Section 5.4 of the main submission. The evaluation results on CIFAR-10 and ImageNet are shown in Table 21. As shown in Table 21: 1) the clean model obtains the best clean accuracy while poorest robustness under most attacks; 2) RND can improve the defense performance of clean model on both datasets. Yet the random noise induced by RND will also sacrifice the clean accuracy. 3) GT provides a better protection of clean accuracy under the random noise induced by RND, so we can adopt a relative larger $\nu = 0.05$ for RND-GT towards better defense performance. RNG-GT can significantly improve the defense performance under all attack methods while maintaining a satisfactory clean performance. Similar to the results of ℓ_∞ attack in the main submission, compared with RSE, PNI, and Feature Denoise (FD), RND-GF achieves the better defense effect against Bandit, SimBA, and ZS and maintain the much better clean accuracy and low training cost. Combining AT with RND, RND-AT significantly improves the robustness against all attacks and achieves best performance among all methods.

Table 21: The comparison of RND ($\nu = 0.02$), GF, RND-GF ($\nu = 0.05$), AT, RND-AT ($\nu = 0.05$), PNI, RSE, and FD on CIFAR-10 and Imagenet. The average number of queries of successful attack and the attack failure rates are reported. The best and second best attack failure rate under each attack are highlighted in bold and underlined respectively.

Datasets	Methods	Clean Acc	NES(ℓ_2)	ZS(ℓ_2)	Bandit(ℓ_2)	SimBA(ℓ_2)	Square(ℓ_2)
CIFAR-10 (WideNet-28)	Clean Model	**96.60%**	729.1/0.025	967.4/0.224	619.0/0.03	457.2/0.04	631.3/0.03
	RND	93.60%	1279.7/0.194	1476.1/0.446	1624.1/0.762	2112.6/0.549	1221.5/0.487
	GF	91.72%	967.4/0.595	826.4/0.645	1543.5/0.274	1146.8/0.395	1626.5/0.328
	RND-GF	92.40%	3209.8/0.661	2453.2/0.901	1362.1/0.838	1220.2/0.863	1415.3/0.692
	RSE	84.12%	1293.6/0.387	1367.9/0.391	264.5/0.334	498.3/0.337	599.0/0.231
	PNI	87.20%	1457.1/0.812	1939.5/0.843	897.9/0.861	945.0/0.857	485.2/0.826
	AT	89.48%	1155.4/0.765	397.5/0.856	2163.2/0.588	1523.2/0.635	1935.4/0.677
	RND-AT	87.40%	3044.4/**0.849**	2904.0/**0.956**	1603.5/**0.931**	1787.4/**0.912**	1292.8/**0.842**
ImageNet (ResNet-50)	Clean Model	**74.90%**	1335.6/0.03	1254.2/0.216	856.0/0.0	1234.5/0.281	621.1/0.01
	RND	73.00%	2027.8/0.509	2566.1/0.631	312.4/0.764	825.3/0.612	1563.1/0.481
	GF	74.70%	1803.7/0.146	1902.1/0.194	896.3/0.056	1417.4/0.112	915.7/0.042
	RND-GF	71.15%	1542.7/0.760	1625.5/0.820	511.4/0.875	777.2/ 0.829	1130.2/0.625
	FD	54.20%	2048.4/0.724	709.3/0.812	2605.9/0.545	2607.9/0.613	1539.1/0.482
	AT	61.60%	2365.1/0.782	639.3/0.912	2769.2/0.544	2638.2/0.651	1404.3/0.528
	RND-AT	58.15%	2482.9/**0.926**	2395.4/**0.937**	1079.1/**0.935**	1210.5/**0.953**	175.0/**0.80**

B.7 The Comparison with Input Transformation-based Defense Methods

Apart from the compared randomization-based methods in main submission, we also compare RND with input transformation-based defense methods, R&P [25], JPEG [10], and Bit-Red [27]. We take the comparison on the ImageNet and Inception-v3 model. We adopt the NES, SignHunter, and Square attacks. The maximal query number is 10000. For RND, we set the ν as 0.02. We report the ℓ_∞ attack results. The results *w.r.t.* the standard attack and the adaptive EOT attack with $M = 5$ are given below tables. Compared to these input transformation-based defense methods, RND achieves better results in both clean accuracy and defense performance.

Table 22: The evaluation of RND, R&P, JPEG, and Bit-Red against ℓ_∞ attack on ImageNet and Inception-v3 model. We adopt NES, SignHunter, and Square attacks. Each value in this table means the average number of query of successful attack and attack failure rate

Defense Methods	clean accuracy	NES(ℓ)	SignHunter(ℓ)	Square(ℓ)
R&P	74.6%	1368.2/0.378	345.1/0.223	285.8/0.153
Bit-Red	62.5%	1548.6/0.092	145.4/0.048	356.2/0.021
JPEG	74.2%	1417.4/0.205	156.8/0.146	215.3/0.033
RND	76.6%	2143.4/0.413	173.4/0.532	251.7/0.207

Table 23: The evaluation of RND, R&P, JPEG, and Bit-Red against ℓ_∞ EOT attack ($M = 5$) on ImageNet and Inception-v3 model. We adopt NES, SignHunter, and Square attacks. Each value in this table means the average number of query of successful attack and attack failure rate

Defense Methods	clean accuracy	NES(ℓ)	SignHunter(ℓ)	Square(ℓ)
R&P	74.6%	2547.6/0.302	545.6/0.148	656.2/0.069
Bit-Red	62.5%	12682.3/0.031	612.3/0.010	689.3/0.004
JPEG	74.2%	2863.2/0.117	485.6/0.094	712.5/0.009
RND	76.6%	3240.2/0.365	336.5/0.456	0.9/0.121

C Analysis and Evaluation of Decision-based Attacks

In this section, we give the analysis of defense effect of RND against decision-based attacks.

For decision-based attacks, the attacker only obtain the classification label by querying the attacked models. As mentioned in main submission, score-based attacks utilize the gradient estimation or random search to find adversarial direction from the benign example to adversarial example with wrong label. However, decision-based attack adopt the different idea to find adversarial examples. Compared with score-based attacks, decision-based attacks first add the large perturbation which make true the found examples in the initial phase can be misclassified. Then, to satisfy the requirement of perturbation size, the attackers need to reduce the distance between found example and the benign example and still have to make sure that the found example can be misclassified. Therefore, the decision-based attacks conduct attacks from adversarial example with large perturbation to benign examples. The found adversarial examples will eventually fall near the boundary [3, 4, 5, 6, 7, 9].

Decision-based attacks can be also separated into gradient estimation and random search-based attacks. Gradient estimation attacks contain Sign-OPT attack [9] and OPT attack [7], and HopSkipJumpAttack (HSJA) [4]. search-based attacks contain boundary attack [3], Sign Flip [6] and RayS [5]. To find the adversarial examples near the decision boundary, binary search is widely used in these two methods. Then, **gradient estimation [4, 7, 9] or random search [5, 6] are conducted to find attack direction near the decision boundary**. Therefore, our analysis about ZO attacks and random search still apply to decision attacks.

We conduct the evaluation of RND against decision-based attacks to verify our analysis. We evaluate Sign-OPT attack, HSJA, Sign Flip, and Rays, because these four attack methods show the better attack performance. We report the performance of RND on WideNet-28-10 and CIFAR-10. We also utilize the Gaussian augmentation fine-tuning to fine the WideNet-28. The work in [4, 5, 6] adopt the fixed size schedule. Therefore, we only tune the noise size μ of Sign-OPT attack like NES [16], zosignsgd [18], Bandit [17], and Square attack [2]. The clean accuracy under different noise has shown in main submission. The experiments results are shown in next tables.

The results in below tables show that: the attack failure rate of attack methods generally increases as the value of $\frac{\nu}{\mu}$ increases. These collaborate our theoretical analysis that **the ratio of $\frac{\nu}{\mu}$ determines the probability of changing sign and the convergence rate of ZO attacks.** The larger $\frac{\nu}{\mu}$, the higher the probability of changing the sign and the convergence error of ZO attacks, which results in the poor attack performance of decision-based attacks under the query-limited settings.

As shown in the below tables, RND can significant boost the defense performance of the Clean Model against the decision-based attacks. Based on GF, RNG-GF further improves the defense performance under all attack methods while maintaining the good clean accuracy.

Table 24: The experimental results of Sign-OPT ℓ_∞ attack on CIFAR-10, WideNet-28 model. Each value in this table means the average number of query of successful attack, and failure rate $\in [0, 1]$.

Methods \ μ/ν	$0.01/0.0$	$0.01/0.01$	$0.01/0.02$	$0.05/0.0$	$0.05/0.01$	$0.05/0.02$	$0.1/0.0$	$0.1/0.01$	$0.1/0.02$
Sign-OPT (RND)	1999.5/0.028	1205.2/0.929	1008.7/0.935	2153.5/0.034	1235.2/0.890	1428.6/0.926	2477.6/0.044	1820.3/0.870	1959.6/0.921

Table 25: The experimental results of HSJA, Sing Flip, and RayS attacks under ℓ_∞ norm on CIFAR-10, WideNet-28 model. Each value in this table means the average number of query of successful attack, and failure rate $\in [0, 1]$.

Methods \ ν	0.0	0.01	0.02
HSJA (ℓ_∞)	977.7/ 0.002	2792.6/0.593	3370.8/0.623
Sign Flip (ℓ_∞)	222.1/0.0	1095.0/0.360	564.4/0.540
RayS (ℓ_∞)	685.9/0.0	998.7/0.06	865.6/0.210

Table 26: The experimental results of Sign-OPT ℓ_∞ attack on CIFAR-10, WideNet-28 GF model. Each value in this table means the average number of query of successful attack, and failure rate $\in [0, 1]$.

Methods \ μ/ν	$0.01/0.0$	$0.01/0.02$	$0.01/0.05$	$0.05/0.0$	$0.05/0.02$	$0.05/0.05$	$0.1/0.0$	$0.1/0.02$	$0.1/0.05$
Sign-OPT (RND-GF)	3257.6/0.651	2217.3/0.783	541.6/0.961	2950.4/0.670	2017.1/0.735	641.5/0.961	3969.1/0.682	1516.4/0.716	465.2/0.938

Table 27: The experimental results of HSJA, Sing Flip, and RayS attacks under ℓ_∞ norm on CIFAR-10, WideNet-28 GF model. Each value in this table means the average number of query of successful attack, and failure rate $\in [0, 1]$.

Methods \ ν	0.0	0.02	0.05
HSJA (ℓ_∞)	4629.8/0.11	4878.5/0.795	6177.2/0.952
Sign Flip (ℓ_∞)	2337.9/ 0.115	3134.9/0.736	1565.6/0.961
RayS (ℓ_∞)	1303.5/0.034	314.6/0.324	572.8/0.564

Table 28: The experimental results of Sign-OPT ℓ_∞ attack on ImageNet, Inception v3 model. Each value in this table means the average number of query of successful attack, and failure rate $\in [0, 1]$.

Methods \ μ/ν	$0.01/0.0$	$0.01/0.01$	$0.01/0.02$	$0.05/0.0$	$0.05/0.01$	$0.05/0.02$	$0.1/0.0$	$0.1/0.01$	$0.1/0.02$
Sign-OPT (RND)	6901.5/0.174	2512.6/0.912	1903.5/0.976	6432.6/0.243	2465.6/0.884	1963.1/0.931	7602.5/0.391	2278.6/0.842	2603.4/0.926

Table 29: The experimental results of HSJA, Sing Flip, and RayS attacks under ℓ_∞ norm on ImageNet, Inception v3 model. Each value in this table means the average number of query of successful attack, and failure rate $\in [0, 1]$.

Methods \ ν	0.0	0.01	0.02
HSJA (ℓ_∞)	2912.9/ 0.150	3289.2/0.791	3370.8/0.879
Sign Flip (ℓ_∞)	2216.1/0.105	1485.2/0.756	1400.6/0.864
RayS (ℓ_∞)	1321.5/0.067	947.2/0.284	787.2/0.326

D Proof of Section 4.2.1

We first give some function properties we will use in next sections:

Definition 1. *The Gaussian-Smoothing function corresponding to $f(\boldsymbol{x})$ with $\alpha > 0$ is defined as follows*

$$f_\alpha(\boldsymbol{x}) = \frac{1}{(2\pi)^{d/2}} \int f(\boldsymbol{x} + \alpha \boldsymbol{a}) \cdot \mathrm{e}^{-\frac{1}{2}\|\boldsymbol{a}\|_2^2} \, \mathrm{d}\boldsymbol{a}. \tag{1}$$

Here, $\alpha \geq 0$ is the smoothing parameter. And if f is convex and the subgradient $\boldsymbol{g} \in \partial f(\boldsymbol{x})$, then

$$f_\mu(\boldsymbol{x}) \geq \frac{1}{(2\pi)^{d/2}[\det \boldsymbol{\Sigma}]^{d/2}} \int [f(\boldsymbol{x}) + \mu \langle \boldsymbol{g}, \boldsymbol{u} \rangle] \mathrm{e}^{-\frac{1}{2}\|\boldsymbol{u}\|^2} \, \mathrm{d}\boldsymbol{u} = f(\boldsymbol{x})$$

If $f \in C^{0,0}$, then $f_\mu \in C^{0,0}$ and $L_0(f_\mu) \leq L_0(f)$. Indeed, for all $x, y \in R^d$ we have

$$\begin{aligned} |f_\mu(x) - f_\mu(y)| &\leq \frac{1}{(2\pi)^{d/2}[\det \boldsymbol{\Sigma}]^{d/2}} \int |f(x + \mu u) - f(y + \mu u)| \mathrm{e}^{-\frac{1}{2}\|u\|^2} \, \mathrm{d}u \\ &\leq L_0(f)\|x - y\| \end{aligned}$$

If $f \in C^{1,1}$, then $f_\mu \in C^{1,1}$ and $L_1(f_\mu) \leq L_1(f)$:

$$\begin{aligned} \|\nabla f_\mu(x) - \nabla f_\mu(y)\| &\leq \frac{1}{(2\pi)^{d/2}[\det \boldsymbol{\Sigma}]^{d/2}} \int_E \|\nabla f(x + \mu u) - \nabla f(y + \mu u)\| \mathrm{e}^{-\frac{1}{2}\|u\|^2} \, \mathrm{d}u \\ &\leq L_1(f)\|x - y\| \end{aligned}$$

For the gradients of $f_\mu(x)$,

$$\begin{aligned} f_\mu(\boldsymbol{x}) &= \frac{1}{\mu^{d+1}(2\pi)^{d/2}[\det \boldsymbol{\Sigma}]^{d/2}} \int f(\boldsymbol{y}) \mathrm{e}^{-\frac{1}{2\mu^2}\|\boldsymbol{y} - \boldsymbol{x}\|^2} \, \mathrm{d}\boldsymbol{y} \\ \nabla f_\mu(\boldsymbol{x}) &= \frac{1}{\mu^{d+3}(2\pi)^{d/2}[\det \boldsymbol{\Sigma}]^{d/2}} \int f(\boldsymbol{y}) \mathrm{e}^{-\frac{1}{2\mu^2}\|\boldsymbol{y} - \boldsymbol{x}\|^2} (\boldsymbol{y} - \boldsymbol{x}) \mathrm{d}\boldsymbol{y} \\ &= \frac{1}{\mu(2\pi)^{d/2}[\det \boldsymbol{\Sigma}]^{d/2}} \int f(\boldsymbol{x} + \mu \boldsymbol{u}) \mathrm{e}^{-\frac{1}{2}\|\boldsymbol{u}\|^2} \boldsymbol{u} \, \mathrm{d}\boldsymbol{u} \\ &= \frac{1}{(2\pi)^{d/2}[\det \boldsymbol{\Sigma}]^{d/2}} \int \frac{f(\boldsymbol{x} + \mu \boldsymbol{u}) - f(\boldsymbol{x})}{\mu} \mathrm{e}^{-\frac{1}{2}\|\boldsymbol{u}\|^2} \boldsymbol{u} \, \mathrm{d}\boldsymbol{u} \end{aligned}$$

We can see that the gradient estimator g_μ is the unbiased estimator of $\nabla f_\mu(\boldsymbol{x})$. Denote by $f'(\boldsymbol{x}, \boldsymbol{u})$ the directional derivative of f at point $\boldsymbol{x}$ along direction $\boldsymbol{u}$:

$$\begin{aligned} f'(\boldsymbol{x}, \boldsymbol{u}) &= \langle \nabla f(\boldsymbol{x}), \boldsymbol{u} \rangle = \lim_{\mu \downarrow 0} \frac{1}{\mu}[f(\boldsymbol{x} + \mu \boldsymbol{u}) - f(\boldsymbol{x})] \\ \nabla f(\boldsymbol{x}) &= \frac{1}{(2\pi)^{d/2}[\det \boldsymbol{\Sigma}]^{d/2}} \int f'(\boldsymbol{x}, \boldsymbol{u}) \mathrm{e}^{-\frac{1}{2}\|\boldsymbol{u}\|^2} \boldsymbol{u} \, \mathrm{d}\boldsymbol{u} \end{aligned}$$

Next, we give some essential lemmas. The complete proofs are shown in [21].

Lemma 1. *Let f be the Lipschitz-continuous function, $|f(\boldsymbol{y}) - f(\boldsymbol{x})| \leq L_0(f)\|\boldsymbol{y} - \boldsymbol{x}\|$. Then*

$$L_1(f_\mu) = \frac{d^{\frac{1}{2}}}{\mu} L_0(f)$$

Lemma 2. *For the smoothed version f_μ of f, if both of them has Lipschitz-continuous gradient, then*

$$L_1(f_\mu) \leq L_1(f)$$

And we define the p-order moment of normal distribution as M_p. We need the upper bound for moment of standard Gaussian distribution.

Lemma 3. *For $p \in [0, 2]$, we have*

$$M_p \leq d^{p/2}$$

If $p \geq 2$, then we have two-side bounds

$$d^{p/2} \leq M_p \leq (p + d)^{p/2}$$

D.1 The General Non-Convex Case

Recalling the optimization problem for attacker:

$$\begin{aligned} &\min_{\boldsymbol{x}_{adv}} f(\boldsymbol{x}_{adv}) \\ &St.\ \|\boldsymbol{x}_{adv} - \boldsymbol{x}\|_p \leq R \end{aligned}$$

The gradient estimator $g(\boldsymbol{x})$ in ZO attacks becomes

$$g_{\mu,\nu}(\boldsymbol{x}) = \frac{f\left(\boldsymbol{x} + \mu\boldsymbol{u} + \nu\boldsymbol{v}_1\right) - f\left(\boldsymbol{x} + \nu\boldsymbol{v}_2\right)}{\mu}\boldsymbol{u} \tag{2}$$

Here, **we use Euclidean norm in our all theoretical analysis**.

We firstly define

$$f_{\mu,\nu}(\boldsymbol{x}) = \frac{1}{(2\pi)^{d/2}} \int f_\nu(\boldsymbol{x} + \mu\boldsymbol{u}) \mathrm{e}^{-\frac{1}{2}\|\boldsymbol{u}\|^2}\, \mathrm{d}\boldsymbol{u}$$

which is the smoothing version of $f_\nu(\boldsymbol{x})$.

We denote the sequence of standard Gaussian noises added by the attacker as $\boldsymbol{\mathcal{U}}_t = \{\boldsymbol{u}_0, \boldsymbol{u}_1, \ldots, \boldsymbol{u}_t\}$. The sequence of standard Gaussian noises added by the defender is denoted as $\boldsymbol{\mathcal{V}}_t = \{\boldsymbol{v}_{01}, \boldsymbol{v}_{02}, \ldots, \boldsymbol{v}_{t1}, \boldsymbol{v}_{t2}\}$. The sequential solutions generated are denoted as $\{\boldsymbol{x}_0, \boldsymbol{x}_1, \ldots, \boldsymbol{x}_Q\}$, and the benign example $\boldsymbol{x}$ is used as the initial solution, $\boldsymbol{x}_0 = \boldsymbol{x}$. $d = |\mathcal{X}|$ denotes the input dimension.

Then we give the proof of Theorem 1.

Proof. According to the Lemma 1, f is the Lipschitz-continuous function, f_ν has the Lipschitz-continuous gradient. So, according to the property of Lipschitz-continuous gradient,

$$f_{\mu,\nu}(\boldsymbol{x}_{t+1}) \leq f_{\mu,\nu}(\boldsymbol{x}_t) - \eta_t\langle \nabla f_{\mu,\nu}(\boldsymbol{x}_t), g_{\mu,\nu}(\boldsymbol{x}_t)\rangle + \frac{1}{2}\eta_t^2 L_1(f_{\mu,\nu})\|g_{\mu,\nu}(\boldsymbol{x}_t)\|^2 \tag{3}$$

The $g_{\mu,\nu}(\boldsymbol{x}_t)$ can be decomposed into

$$\begin{aligned} g_{\mu,\nu}(\boldsymbol{x}_t) &= g_\mu(\boldsymbol{x}_t + \nu\boldsymbol{v}_{t1}) + \frac{f(\boldsymbol{x}_t + \mu\boldsymbol{u_t} + \nu\boldsymbol{v}_{t1}) - f(\boldsymbol{x}_t + \nu\boldsymbol{v}_{t1}) + f(\boldsymbol{x}_t + \nu\boldsymbol{v}_{t1}) - f(\boldsymbol{x}_t + \nu\boldsymbol{v}_{t2})}{\mu}\boldsymbol{u}_t \\ &\geq g_\mu(\boldsymbol{x}_t + \nu\boldsymbol{v}_{t1}) - \frac{L_0(f)\nu\|\boldsymbol{v}_{t1} - \boldsymbol{v}_{t2}\|\boldsymbol{u}_t}{\mu} \end{aligned} \tag{4}$$

And, following the above decomposition Eq.(4), the last square term of Eq.(3) is bounded by

$$\begin{aligned} \|g_{\mu,\nu}(\boldsymbol{x}_t)\|^2 \leq &\frac{(f(\boldsymbol{x}_t + \mu\boldsymbol{u_t} + \nu\boldsymbol{v}_{t1}) - f(\boldsymbol{x}_t + \nu\boldsymbol{v}_{t1}))^2\|\boldsymbol{u_t}\|^2}{\mu^2} + \frac{(f(\boldsymbol{x}_t + \nu\boldsymbol{v}_{t1}) - f(\boldsymbol{x}_t + \nu\boldsymbol{v}_{t2}))^2\|\boldsymbol{u_t}\|^2}{\mu^2} \\ &+ \frac{2|f(\boldsymbol{x}_t + \mu\boldsymbol{u_t} + \nu\boldsymbol{v}_{t1}) - f(\boldsymbol{x}_t + \nu\boldsymbol{v}_{t1})| * |f(\boldsymbol{x} + \nu\boldsymbol{v}_{t1}) - f(\boldsymbol{x} + \nu\boldsymbol{v}_{t2})|}{\mu^2}\|\boldsymbol{u_t}\|^2 \\ \leq &\|g_u(\boldsymbol{x} + \nu\boldsymbol{v}_{t1})\|^2 + \frac{L_0(f)^2\nu^2}{\mu^2}\|\boldsymbol{v}_{t1} - \boldsymbol{v}_{t2}\|^2\|\boldsymbol{u_t}\|^2 + 2\frac{L_0(f)^2\nu}{\mu}\|\boldsymbol{v}_{t1} - \boldsymbol{v}_{t2}\|\|\boldsymbol{u_t}\|^3 \end{aligned} \tag{5}$$

Then, we take the expectation over $\boldsymbol{u}_t$, $\boldsymbol{v}_{t1}$ and $\boldsymbol{v}_{t2}$. And since $\boldsymbol{v}_{t1}$ and $\boldsymbol{v}_{t2}$ are identically independent with each other, $\boldsymbol{v}_{t1} - \boldsymbol{v}_{t2}$ is still Gaussian random variable. So, according to Lemma 3, we have

$$\begin{aligned} \mathbb{E}_{u_t, v_{t1,t2}}(f_{\mu,\nu}(\boldsymbol{x}_{t+1})) \leq &f_{\mu,\nu}(\boldsymbol{x}_t) - \eta_t\|\nabla f_{\mu,\nu}(\boldsymbol{x}_t)\|^2 + \frac{1}{2}\eta_t^2 L_1(f_{\mu,\nu})(L_0(f)^2(d+4)^2 \\ &+ \frac{2L_0(f)^2\nu^2}{\mu^2}d^2 + \frac{2\sqrt{2}L_0(f)^2\nu}{\mu}(d+3)^{\frac{3}{2}}d^{\frac{1}{2}}) \end{aligned} \tag{6}$$

And then use Lemma 1, we have $L_1(f_{\mu,\nu}) \leq L_0(f_\nu) \leq L_0(f)$, so

$$\begin{aligned} \mathbb{E}_{u_t, v_{t1,t2}}(f_{\mu,\nu}(\boldsymbol{x}_{t+1})) \leq &f_{\mu,\nu}(\boldsymbol{x}_t) - \eta_t\|\nabla f_{\mu,\nu}(\boldsymbol{x}_t)\|^2 + \frac{1}{2}\eta_t^2\frac{L_0(f)^3}{\mu}(d+4)^2 d^{\frac{1}{2}} \\ &+ \eta_t^2\frac{L_0(f)^3\nu^2}{\mu^3}d^{\frac{5}{2}} + \eta_t^2\frac{\sqrt{2}L_0(f)^3\nu}{\mu^2}(d+3)^{\frac{3}{2}}d \end{aligned}$$

We take the expectation on $\mathcal{U}_t$, $\mathcal{V}_t$ and

$$\begin{aligned}\mathbb{E}_{\mathcal{U}_t,\mathcal{V}_t}(f_{\mu,\nu}(\boldsymbol{x}_{t+1})) \leq & \mathbb{E}_{\mathcal{U}_{t-1},\mathcal{V}_{t-1}}(f_{\mu,\nu}(\boldsymbol{x}_t)) - \eta_t \mathbb{E}_{\mathcal{U}_t,\mathcal{V}_t}(\|\nabla f_{\mu,\nu}(\boldsymbol{x}_t)\|^2) + \frac{1}{2}\eta_t^2 \frac{L_0(f)^3}{\mu}(d+4)^2 d^{\frac{1}{2}} \\ & + \eta_t^2 \frac{L_0(f)^3 \nu^2}{\mu^3} d^{\frac{5}{2}} + \eta_t^2 \frac{\sqrt{2} L_0(f)^3 \nu}{\mu^2}(d+3)^{\frac{3}{2}} d\end{aligned}$$

For our black-box attacks problem, data dimension is very high ($10^5 \sim 10^7$). So, we have

$$\begin{aligned}\mathbb{E}_{\mathcal{U}_t,\mathcal{V}_t}(f_{\mu,\nu}(\boldsymbol{x}_{t+1})) \leq & \mathbb{E}_{\mathcal{U}_{t-1},\mathcal{V}_{t-1}}(f_{\mu,\nu}(\boldsymbol{x}_t)) - \eta_t \mathbb{E}_{\mathcal{U}_t,\mathcal{V}_t}(\|\nabla f_{\mu,\nu}(\boldsymbol{x}_t)\|^2) \\ & + \eta_t^2 L_0(f)^3 d^{\frac{5}{2}} (\frac{1}{2\mu} + \frac{\sqrt{2}\nu}{\mu^2} + \frac{\nu^2}{\mu^3})\end{aligned}$$

Using the same reasoning, we get

$$\begin{aligned}\mathbb{E}_{\mathcal{U}_0,\mathcal{V}_0}(f_{\mu,\nu}(\boldsymbol{x}_1)) \leq & (f_{\mu,\nu}(\boldsymbol{x}_0)) - \eta_t \mathbb{E}_{\mathcal{U}_0,\mathcal{V}_0}(\|\nabla f_{\mu,\nu}(\boldsymbol{x}_0)\|^2) \\ & + \eta_t^2 L_0(f)^3 d^{\frac{5}{2}} (\frac{1}{2\mu} + \frac{\sqrt{2}\nu}{\mu^2} + \frac{\nu^2}{\mu^3})\end{aligned}$$

Summing up these inequalities, denote $S_Q = \sum_{t=0}^{Q} \eta_t$. And according to the property $f_\mu(\boldsymbol{x}) \geq f(\boldsymbol{x})$, we also have $f_{\mu,\nu}(\boldsymbol{x}) \geq f_\nu(\boldsymbol{x})$. So we get

$$\frac{1}{S_Q}\sum_{t=0}^{Q} \eta_t \mathbb{E}_{\mathcal{U}_t,\mathcal{V}_t}(\|\nabla f_{\mu,\nu}(\boldsymbol{x}_t)\|^2) \leq \frac{1}{S_Q}(f_{\mu,\nu}(\boldsymbol{x}_0) - f_\nu^*) + \frac{1}{S_Q}\sum_{t=0}^{Q} \eta_t^2 L_0(f)^3 d^{\frac{5}{2}} (\frac{1}{2\mu} + \frac{\sqrt{2}\nu}{\mu^2} + \frac{\nu^2}{\mu^3})$$

Here, in order to bound the gap ϵ between $f_{\mu,\nu}(x)$ and $f_\nu(x)$, we could choose $\mu \leq \hat{\mu} = \frac{\epsilon}{d^{\frac{1}{2}} L_0(f)}$ like without adding noise [21]. So we have

$$\frac{1}{S_Q}\sum_{t=0}^{Q} \eta_t \mathbb{E}_{\mathcal{U}_t,\mathcal{V}_t}(\|\nabla f_{\mu,\nu}(\boldsymbol{x}_t)\|^2) \leq \frac{1}{S_Q}(f_{\mu,\nu}(\boldsymbol{x}_0) - f_\nu^*) + \frac{1}{S_Q}\sum_{t=0}^{Q} \frac{\eta_t^2 L_0(f)^4 d^3}{\epsilon} (\frac{1}{2} + \frac{\sqrt{2}\nu}{\mu} + \frac{\nu^2}{\mu^2})$$

We take the constant stepsize and set $\eta_t = \eta$. We also denote $\alpha = \frac{\nu}{\mu}$. And we set $(\frac{1}{2} + \sqrt{2}\alpha + \alpha^2)$ as $\gamma(\alpha)$ which is increasing function of the ratio $\frac{\nu}{\mu}$. We minimize the right hand side then get

$$\eta = \left[\frac{R\epsilon}{d^3 L_0^3(f)(Q+1)}\right]^{1/2} \frac{1}{\sqrt{\gamma(\alpha)}}$$

So we can get

$$\frac{1}{Q+1}\sum_{t=0}^{Q} \mathbb{E}_{\mathcal{U}_{t-1},\mathcal{V}_{t-1}}(\|\nabla f_{\mu,\nu}(\boldsymbol{x}_t)\|^2) \leq \frac{2L_0(f)^{\frac{5}{2}} R^{\frac{1}{2}} d^{\frac{3}{2}}}{(Q+1)^{\frac{1}{2}} \epsilon^{\frac{1}{2}}} \sqrt{\gamma(\alpha)} \tag{7}$$

In order to guarantee the expected squared norm of the gradient of function $f_{\mu,\nu}$ of the order δ, the lower bound for the expected number of queries is

$$O\left(\gamma(\alpha)\frac{d^3 L_0^5(f) R}{\epsilon \delta^2}\right)$$

$\square$

E Proof of Section 4.2.2

E.1 The Non-Convex and Smooth Case

Now, the gradient estimator in ZO attacks becomes

$$\tilde{g}_{\mu,\nu}(\boldsymbol{x}) = \frac{1}{M}\sum_{j=1}^{M} \frac{f(\boldsymbol{x} + \mu\boldsymbol{u} + \nu\boldsymbol{v}_{j1}) - f(\boldsymbol{x} + \nu\boldsymbol{v}_{j2})}{\mu}\boldsymbol{\mu} \tag{8}$$

We denote the sequence of standard Gaussian noises added by the attacker as $\boldsymbol{\mathcal{U}}_t = \{\boldsymbol{u}_0, \boldsymbol{u}_1, \dots, \boldsymbol{u}_t\}$. Note that here the definition of the sequential standard Gaussian noises added by the defende should be updated to $\boldsymbol{\mathcal{V}}_t = \{\boldsymbol{v}_{01}, \dots, \boldsymbol{v}_{0M}, \dots, \boldsymbol{v}_{t1}, \dots, \boldsymbol{v}_{tM}\}$. $\boldsymbol{v}_{ij} \in \boldsymbol{\mathcal{V}}_t$ contains $\boldsymbol{v}_{ij1}$ and $\boldsymbol{v}_{ij2}$.

Then we give the proof of Theorem 2.

Proof. Followed by proof of last section, according to the property of Lipschitz-continuous gradient,

$$f_{\mu,\nu}(\boldsymbol{x}_{t+1}) \leq f_{\mu,\nu}(\boldsymbol{x}_t) - \eta_t \langle \nabla f_{\mu,\nu}(\boldsymbol{x}_t), \tilde{g}_{\mu,\nu}(\boldsymbol{x}_t)\rangle + \frac{1}{2}\eta_t^2 L_1(f_{\mu,\nu}) \|\tilde{g}_{\mu,\nu}(\boldsymbol{x}_t)\|^2 \tag{9}$$

Followed by Eq.(4), the $\tilde{g}_{\mu,\nu}(\boldsymbol{x}_t)$ can be also decomposed into

$$\tilde{g}_{\mu,\nu}(\boldsymbol{x}_t) \geq \sum_{j=1}^{M} \frac{1}{M} g_\mu(\boldsymbol{x}_t + \nu \boldsymbol{v}_{t1j}) - \frac{L_0(f)\nu \|\boldsymbol{v}_{t1} - \boldsymbol{v}_{t2}\| \boldsymbol{u}_t}{\mu} \tag{10}$$

Then, to bound the square term of gradient estimator, we use the decomposition

$$\|\tilde{g}_{\mu,\nu}(\boldsymbol{x}_t)\|^2 = \|g_\mu(\boldsymbol{x}_t)\|^2 + \|(\tilde{g}_{\mu,\nu}(\boldsymbol{x}_t) - g_\mu(\boldsymbol{x}_t))\|^2 + 2\langle g_\mu(\boldsymbol{x}_t), (\tilde{g}_{\mu,\nu}(\boldsymbol{x}_t) - g_\mu(\boldsymbol{x}_t))\rangle \tag{11}$$

So, we have

$$\begin{aligned}
\mathbb{E}_{\boldsymbol{v}_{t1-tM}, \boldsymbol{u}_t}(f_{\mu,\nu}(\boldsymbol{x}_{t+1})) \leq & f_{\mu,\nu}(\boldsymbol{x}_t) - \eta_t \mathbb{E}_{\boldsymbol{v}_{t1-tM}, \boldsymbol{u}_t}(\langle \nabla f_{\mu,\nu}(\boldsymbol{x}_t), \tilde{g}_{\mu,\nu}(\boldsymbol{x}_t)\rangle) \\
& + \frac{1}{2}\eta_t^2 L_1(f_{\mu,\nu}) \mathbb{E}_{\boldsymbol{v}_{t1-tM}, \boldsymbol{u}_t}(\|\tilde{g}_{\mu,\nu}(\boldsymbol{x}_t)\|^2) \\
\leq & f_{\mu,\nu}(\boldsymbol{x}_t) - \eta_t \mathbb{E}_{\boldsymbol{v}_{t1-tM}, \boldsymbol{u}_t}(\langle \nabla f_{\mu,\nu}(\boldsymbol{x}_t), \sum_{j=1}^{M} \frac{1}{M} g_\mu(\boldsymbol{x}_t + \nu \boldsymbol{v}_{t1j})\rangle) \\
& + \frac{1}{2}\eta_t^2 L_1(f_{\mu,\nu}) \mathbb{E}_{\boldsymbol{v}_{t1-tM}, \boldsymbol{u}_t}(\|g_\mu(\boldsymbol{x}_t)\|^2 + \|(\tilde{g}_{\mu,\nu}(\boldsymbol{x}_t) - g_\mu(\boldsymbol{x}_t))\|^2 \\
& + 2\langle g_\mu(\boldsymbol{x}_t), (\tilde{g}_{\mu,\nu}(\boldsymbol{x}_t) - g_\mu(\boldsymbol{x}_t))\rangle)
\end{aligned} \tag{12}$$

Since $\boldsymbol{v}_{t1-tM}$ are iid random variables, the second term of above inequality is same as the second term of Eq.(6). Then we need to bound the last square terms.

We set the expectation over $\boldsymbol{v}_{1j}$, $\mathbb{E}_{\boldsymbol{v}_{1j}}(f(\boldsymbol{x}+\mu\boldsymbol{u})+\nu\boldsymbol{v}_{1j})$ as E_1 and $\mathbb{E}_{\boldsymbol{v}_{2j}}(f(\boldsymbol{x}+\nu\boldsymbol{v}_{2j})$ as E_2. And we also set $B_1 = E_1 - f(\boldsymbol{x}+\mu\boldsymbol{u})$ and $B_2 = E_2 - f(\boldsymbol{x})$. We also set $\sigma_1^2 = Var_{\boldsymbol{v}_{1j}}(f(\boldsymbol{x}+\mu\boldsymbol{u}+\nu\boldsymbol{v}_{1j}))$ and $\sigma_2^2 = Var_{\boldsymbol{v}_{2j}}(f(\boldsymbol{x}+\nu\boldsymbol{v}_{2j}))$. Then we bound the second term of above square terms.

$$\begin{aligned}
\mathbb{E}_{\boldsymbol{v}_{t1-tM}}(\|(\tilde{g}_{\mu,\nu}(\boldsymbol{x}_t) - g_\mu(\boldsymbol{x}_t))\|^2) \leq & (B_1^2 + B_2^2 + \frac{\sigma_1^2 + \sigma_2^2}{M} - 2B_1B_2)\frac{1}{\mu^2}\|\boldsymbol{u}\|^2 \\
\leq & (2(B_1^2 + B_2^2) + \frac{\sigma_1^2 + \sigma_2^2}{M})\frac{1}{\mu^2}\|\boldsymbol{u}\|^2
\end{aligned} \tag{13}$$

We can compute this square of sum directly and we need to bound B^2 and σ^2. By using the Taylor expansion of $f(\boldsymbol{x})$,

$$\begin{aligned}
f(\boldsymbol{x}+\mu\boldsymbol{u}+\nu\boldsymbol{v}_{1j}) \leq & f(\boldsymbol{x}+\mu\boldsymbol{u}) + \nabla f(\boldsymbol{x}+\mu\boldsymbol{u})^T \nu \boldsymbol{v}_{1j} + \frac{1}{2}\nu^2 L_1(f)\|\boldsymbol{v}_{1j}\|^2 \\
E_1 \leq & f(\boldsymbol{x}+\mu\boldsymbol{u}) + \frac{1}{2}\nu^2 L_1(f) d \\
B_1 = & E_1 - f(\boldsymbol{x}+\mu\boldsymbol{u}) \leq \frac{1}{2}\nu^2 L_1(f) d \\
B_1 = & E_1 - f(\boldsymbol{x}+\mu\boldsymbol{u}) \geq -\frac{1}{2}\nu^2 L_1(f) d
\end{aligned}$$

So, we have

$$f(\boldsymbol{x}+\mu\boldsymbol{u}+\nu\boldsymbol{v}_{1j}) - f(\boldsymbol{x}+\mu\boldsymbol{u}) - \frac{1}{2}\nu^2 L_1(f) d \leq f(\boldsymbol{x}+\mu\boldsymbol{u}+\nu\boldsymbol{v}_{1j}) - E_1 \leq f(\boldsymbol{x}+\mu\boldsymbol{u}+\nu\boldsymbol{v}_{1j}) - f(\boldsymbol{x}+\mu\boldsymbol{u}) + \frac{1}{2}\nu^2 L_1(f) d$$

Based on the above inequality, we have

$$\begin{aligned}\mathbb{E}_{\boldsymbol{v}_{1j}}((f(\boldsymbol{x}+\mu\boldsymbol{u}+\nu\boldsymbol{v}_{1j})-E_1)^2) \le& 2\mathbb{E}_{\boldsymbol{v}_{1j}}((f(\boldsymbol{x}+\mu\boldsymbol{u}+\nu\boldsymbol{v}_{1j})-f(\boldsymbol{x}+\mu\boldsymbol{u}))^2)+\frac{1}{2}\nu^4L_1(f)^2d^2\\ \sigma_1^2 \le& 2\nu^2L_0(f)^2d+\frac{1}{2}\nu^4L_1(f)^2d^2\end{aligned}$$

Then, the Eq.(13) becomes

$$\begin{aligned}\mathbb{E}_{\boldsymbol{v}_{t1-tM},\boldsymbol{u}}(\|(\tilde{g}_{\mu,\nu}(\boldsymbol{x}_t)-g_\mu(\boldsymbol{x}_t))\|^2) \le& \mathbb{E}_{\boldsymbol{u}}((B_1^2+B_2^2+\frac{\sigma_1^2+\sigma_2^2}{M}-2B_1B_2)\frac{1}{\mu^2}\|\boldsymbol{u}\|^2)\\ \le& \mathbb{E}_{\boldsymbol{u}}((2(B_1^2+B_2^2)+\frac{\sigma_1^2+\sigma_2^2}{M})\frac{1}{\mu^2}\|\boldsymbol{u}\|^2)\\ \le& \frac{\nu^4}{\mu^2}L_1(f)^2d^3+\frac{\nu^4}{\mu^2M}L_1(f)^2d^3+4\frac{\nu^2}{\mu^2M}L_0(f)^2d^2\end{aligned}\tag{14}$$

And the third term of square terms can be bounded by using B and E.

$$\begin{aligned}&2(f(\boldsymbol{x}+\mu u)-f(\boldsymbol{x}))(\sum_{j=1}^{M}(\frac{f(\boldsymbol{x}+\mu\boldsymbol{u}+\nu\boldsymbol{v}_{1j})-f(\boldsymbol{x}+\nu\boldsymbol{v}_{2j})}{M})-f(\boldsymbol{x}+\mu\boldsymbol{u})+f(\boldsymbol{x}))\frac{1}{\mu^2}\|\boldsymbol{u}\|^2\\ &\le 2(f(\boldsymbol{x}+\mu\boldsymbol{u})-f(\boldsymbol{x}))(E_1-E_2-f(\boldsymbol{x}+\mu\boldsymbol{u})+f(\boldsymbol{x}))\frac{1}{\mu^2}\|\boldsymbol{u}\|^2 \text{ \#taking expectation over } \boldsymbol{v}_{t1-tM},\boldsymbol{v}_{2j}\\ &\le 2\frac{L_0(f)\mu\|\boldsymbol{u}\|(B_1-B_2)\|\boldsymbol{u}\|^2}{\mu^2} \text{ \#taking expectation over } \boldsymbol{u}\\ &\le 2\frac{\nu^2}{\mu}L_0(f)L_1(f)d^{\frac{5}{2}}\end{aligned}\tag{15}$$

So, we have

$$\begin{aligned}\mathbb{E}_{\boldsymbol{v}_{t1-tM},\boldsymbol{u}_t}\|\tilde{g}_{\mu,\nu}(\boldsymbol{x}_t)\|^2 \le& L_0(f)^2(d+4)^2+4\frac{\nu^2L_0(f)^2}{\mu^2M}d^2+2\frac{\nu^2L_0(f)L_1(f)}{\mu}d^{\frac{5}{2}}\\ &+\frac{\nu^4L_1(f)^2}{\mu^2}\frac{M+1}{M}d^3\end{aligned}$$

And based on Lemma 2, the Eq.(21) becomes

$$\begin{aligned}\mathbb{E}_{\boldsymbol{v}_{t1-tM},\boldsymbol{u}_t}(f_{\mu,\nu}(\boldsymbol{x}_{t+1})) \le& f_{\mu,\nu}(\boldsymbol{x}_t)-\eta_t\|\nabla f_{\mu,\nu}(\boldsymbol{x}_t)\|^2+\frac{1}{2}\eta_t^2L_1(f_{\mu,\nu})\mathbb{E}_{\boldsymbol{v}_{t1-tM},\boldsymbol{u}_t}(\|\tilde{g}_{\mu,\nu}(\boldsymbol{x}_t)\|^2)\\ \le& f_{\mu,\nu}(\boldsymbol{x}_t)-\eta_t\|\nabla f_{\mu,\nu}(\boldsymbol{x}_t)\|^2+\eta_t^2(\frac{L_0(f)^2L_1(f)}{2}d^2\\ &+\frac{2\nu^2L_0(f)^2L_1(f)}{\mu^2M}d^2+\frac{\nu^2L_0(f)L_1(f)^2}{\mu}d^{\frac{5}{2}}+\frac{\nu^4L_1(f)^3(M+1)}{2\mu^2M}d^3)\end{aligned}\tag{16}$$

We take the expectation on $\mathcal{U}_t$, $\mathcal{V}_t$,

$$\begin{aligned}\mathbb{E}_{\mathcal{U}_t,\mathcal{V}_t}(f_{\mu,\nu}(\boldsymbol{x}_{t+1})) \le& \mathbb{E}_{\mathcal{U}_{t-1},\mathcal{V}_{t-1}}(f_{\mu,\nu}(\boldsymbol{x}_t))-\eta_t\mathbb{E}_{\mathcal{U}_t,\mathcal{V}_t}(\|\nabla f_{\mu,\nu}(\boldsymbol{x}_t)\|^2)+\eta_t^2(\frac{L_0(f)^2L_1(f)}{2}d^2\\ &+\frac{2\nu^2L_0(f)^2L_1(f)}{\mu^2M}d^2+\frac{\nu^2L_0(f)L_1(f)^2}{\mu}d^{\frac{5}{2}}+\frac{\nu^4L_1(f)^3(M+1)}{2\mu^2M}d^3)\end{aligned}\tag{17}$$

Then we can get

$$
\begin{aligned}
\frac{1}{S_Q}\sum_{t=0}^{Q}\eta_t\mathbb{E}_{\mathcal{U}_t,\mathcal{V}_t}(\|\nabla f_{\mu,\nu}(\boldsymbol{x}_t)\|^2) \leq & \frac{1}{S_Q}(f_{\mu,\nu}(\boldsymbol{x}_0) - f_\nu^*) + \frac{1}{S_Q}\sum_{t=0}^{Q}\eta_t^2(\frac{L_0(f)^2L_1(f)}{2}d^2 \\
& + \frac{2\nu^2L_0(f)^2L_1(f)}{\mu^2M}d^2 + \frac{\nu^2L_0(f)L_1(f)^2}{\mu}d^{\frac{5}{2}} \\
& + \frac{\nu^4L_1(f)^3(M+1)}{2\mu^2M}d^3)
\end{aligned} \tag{18}
$$

□

F The Proof of Section 4.3

The direction searching of search-based attacks [1, 2, 8, 13, 20] can be formulated as

$$
\begin{aligned}
s(\boldsymbol{x}) &= \mathbb{I}(f(\boldsymbol{x}+\mu\boldsymbol{u}) - f(\boldsymbol{x}) < 0)\cdot\mu\boldsymbol{u} \\
&= \mathbb{I}(h(\boldsymbol{x}) < 0)\cdot\mu\boldsymbol{u}
\end{aligned} \tag{19}
$$

where $\boldsymbol{u}$ is the direction searching direction sampled from some pre-defined distributions, such as gaussian noise in [8], orthogonal basis in [13] and squared perturbations in [2].

If the attackers take the attack direction $\boldsymbol{u}$ and objective function decreases, then $\boldsymbol{u}$ will be seen as the potential attack direction.

Now, with the RND, the searched direction becomes

$$
\begin{aligned}
s_\nu(\boldsymbol{x}) &= \mathbb{I}(f(\boldsymbol{x}+\mu\boldsymbol{u}+\nu\boldsymbol{v}_1) - f(\boldsymbol{x}+\nu\boldsymbol{v}_2) < 0)\cdot\mu\boldsymbol{u} \\
&= \mathbb{I}(h_\nu(\boldsymbol{x}) < 0)\cdot\mu\boldsymbol{u}
\end{aligned} \tag{20}
$$

We give the Theorem 3 about the probability of Sign$(h(\boldsymbol{x})) \neq$ Sign$(h_\nu(\boldsymbol{x}))$,

$$
\begin{aligned}
P(\text{Sign}(h(\boldsymbol{x})) \neq \text{Sign}(h_\nu(\boldsymbol{x})) &\leq P(h_\nu(\boldsymbol{x}) - h(\boldsymbol{x})| \geq |h(\boldsymbol{x})|) \\
&\leq \frac{\mathbb{E}[|h_\nu(\boldsymbol{x}) - h(\boldsymbol{x})|]}{|h(\boldsymbol{x})|} \text{ according to the Markov's inequality} \\
&\leq \frac{\sqrt{\mathbb{E}[(h_\nu(\boldsymbol{x}) - h(\boldsymbol{x}))^2]}}{|h(\boldsymbol{x})|} \text{ according to the Jensen's inequality} \\
&\leq \frac{\sqrt{\mathbb{E}[2(f(\boldsymbol{x}+\mu\boldsymbol{u}+\nu\boldsymbol{v}_1) - f(\boldsymbol{x}+\mu\boldsymbol{u}))^2 + 2(f(\boldsymbol{x}+\nu\boldsymbol{v}_2) - f(\boldsymbol{x}))^2]}}{|h(\boldsymbol{x})|} \\
&\leq \frac{\sqrt{\mathbb{E}[2L_0(f)^2\nu^2\|\boldsymbol{v}_1\|^2 + 2L_0(f)^2\nu^2\|\boldsymbol{v}_2\|^2]}}{|h(\boldsymbol{x})|} \text{ according to Lipchitzness of function} \\
&\leq \frac{2L_0(f)\nu\sqrt{d}}{|h(\boldsymbol{x})|} \text{ according to Lemma 3}
\end{aligned} \tag{21}
$$

References

[1] Abdullah Al-Dujaili and Una-May O'Reilly. Sign bits are all you need for black-box attacks. In *International Conference on Learning Representations*, 2020.

[2] Maksym Andriushchenko, Francesco Croce, Nicolas Flammarion, and Matthias Hein. Square attack: a query-efficient black-box adversarial attack via random search. In *European Conference on Computer Vision*, pages 484–501. Springer, 2020.

[3] Wieland Brendel, Jonas Rauber, and Matthias Bethge. Decision-based adversarial attacks: Reliable attacks against black-box machine learning models. In *International Conference on Learning Representations*, 2018.

[4] Jianbo Chen, Michael I Jordan, and Martin J Wainwright. Hopskipjumpattack: A query-efficient decision-based attack. In *2020 ieee symposium on security and privacy (sp)*, pages 1277–1294. IEEE, 2020.

[5] Jinghui Chen and Quanquan Gu. Rays: A ray searching method for hard-label adversarial attack. In *Proceedings of the 26th ACM SIGKDD International Conference on Knowledge Discovery & Data Mining*, pages 1739–1747, 2020.

[6] Weilun Chen, Zhaoxiang Zhang, Xiaolin Hu, and Baoyuan Wu. Boosting decision-based black-box adversarial attacks with random sign flip. In *European Conference on Computer Vision*, pages 276–293. Springer, 2020.

[7] Minhao Cheng, Thong Le, Pin-Yu Chen, Huan Zhang, JinFeng Yi, and Cho-Jui Hsieh. Query-efficient hard-label black-box attack: An optimization-based approach. In *International Conference on Learning Representations*, 2019.

[8] Minhao Cheng, Simranjit Singh, Patrick Chen, Pin-Yu Chen, Sijia Liu, and Cho-Jui Hsieh. Sign-opt: A query-efficient hard-label adversarial attack. *arXiv preprint arXiv:1909.10773*, 2019.

[9] Minhao Cheng, Simranjit Singh, Patrick H. Chen, Pin-Yu Chen, Sijia Liu, and Cho-Jui Hsieh. Sign-opt: A query-efficient hard-label adversarial attack. In *International Conference on Learning Representations*, 2020.

[10] Gintare Karolina Dziugaite, Zoubin Ghahramani, and Daniel M Roy. A study of the effect of jpg compression on adversarial images. *arXiv preprint arXiv:1608.00853*, 2016.

[11] Logan Engstrom, Andrew Ilyas, Hadi Salman, Shibani Santurkar, and Dimitris Tsipras. Robustness (python library), 2019.

[12] Sven Gowal, Chongli Qin, Jonathan Uesato, Timothy Mann, and Pushmeet Kohli. Uncovering the limits of adversarial training against norm-bounded adversarial examples. *arXiv preprint arXiv:2010.03593*, 2020.

[13] Chuan Guo, Jacob Gardner, Yurong You, Andrew Gordon Wilson, and Kilian Weinberger. Simple black-box adversarial attacks. In *International Conference on Machine Learning*, pages 2484–2493, 2019.

[14] Zhezhi He, Adnan Siraj Rakin, and Deliang Fan. Parametric noise injection: Trainable randomness to improve deep neural network robustness against adversarial attack. In *Proceedings of the IEEE Conference on Computer Vision and Pattern Recognition*, pages 588–597, 2019.

[15] Zhichao Huang and Tong Zhang. Black-box adversarial attack with transferable model-based embedding. In *International Conference on Learning Representations*, 2019.

[16] Andrew Ilyas, Logan Engstrom, Anish Athalye, and Jessy Lin. Black-box adversarial attacks with limited queries and information. In *International Conference on Machine Learning*, pages 2137–2146, 2018.

[17] Andrew Ilyas, Logan Engstrom, and Aleksander Madry. Prior convictions: Black-box adversarial attacks with bandits and priors. In *International Conference on Learning Representations*, 2018.

[18] Sijia Liu, Pin-Yu Chen, Xiangyi Chen, and Mingyi Hong. signsgd via zeroth-order oracle. In *International Conference on Learning Representations*, 2018.

[19] Xuanqing Liu, Minhao Cheng, Huan Zhang, and Cho-Jui Hsieh. Towards robust neural networks via random self-ensemble. In *Proceedings of the European Conference on Computer Vision (ECCV)*, pages 369–385, 2018.

[20] Seungyong Moon, Gaon An, and Hyun Oh Song. Parsimonious black-box adversarial attacks via efficient combinatorial optimization. In *International Conference on Machine Learning*, pages 4636–4645. PMLR, 2019.

[21] Yurii Nesterov and Vladimir Spokoiny. Random gradient-free minimization of convex functions. *Foundations of Computational Mathematics*, 17(2):527–566, 2017.

[22] Adam Paszke, Sam Gross, Francisco Massa, Adam Lerer, James Bradbury, Gregory Chanan, Trevor Killeen, Zeming Lin, Natalia Gimelshein, Luca Antiga, et al. Pytorch: An imperative style, high-performance deep learning library. *Advances in Neural Information Processing Systems*, 32:8026–8037, 2019.

[23] Evgenia Rusak, Lukas Schott, Roland S Zimmermann, Julian Bitterwolf, Oliver Bringmann, Matthias Bethge, and Wieland Brendel. A simple way to make neural networks robust against diverse image corruptions. In *European Conference on Computer Vision*, pages 53–69. Springer, 2020.

[24] Leslie N Smith. Cyclical learning rates for training neural networks. In *2017 IEEE winter conference on applications of computer vision (WACV)*, pages 464–472. IEEE, 2017.

[25] Cihang Xie, Jianyu Wang, Zhishuai Zhang, Zhou Ren, and Alan Yuille. Mitigating adversarial effects through randomization. In *International Conference on Learning Representations*, 2018.

[26] Cihang Xie, Yuxin Wu, Laurens van der Maaten, Alan L Yuille, and Kaiming He. Feature denoising for improving adversarial robustness. In *Proceedings of the IEEE/CVF Conference on Computer Vision and Pattern Recognition*, pages 501–509, 2019.

[27] Weilin Xu, David Evans, and Yanjun Qi. Feature squeezing: Detecting adversarial examples in deep neural networks. *Proceedings 2018 Network and Distributed System Security Symposium*, 2018.